SUPPLEMENTARY INFORMATION

Supplementary Table 1

Paleosol	Age (Ga)	Lower age constraint	Upper age constraint	Paleolatitude estimate	Parent	Data source
Basal Pongola	3.0	3,105±3 Ma zircon U-Pb age in parent	2,980±10 Ma youngest detrital zircon U-Pb age in overlying Nsuze Group	27-33° (Luskin et al., 2019)	Granodiorite	New, ICP-MS
Denny Dalton	2.96-2.87	2,968±6 Ma zircon U-Pb age in parent	2,866±2 Ma baddeleyite U-Pb age in crosscutting Hlagothi Complex[1]	NA (age uncertain)	Basaltic andesite (Nsuze Group)	New, ICP-MS
Lake Voronye	2.81	2,795±19 Ma zircon U-Pb age in parent	2,807±3 Ma zircon U-Pb age in overlying andesite (Okhta Sequence)	NA (not available)	Granite	Alfimova et al. (2011), XRF
Mt. Roe #2	2.76	2,763±8 Ma zircon U-Pb age in underlying basalt	2,760±10 Ma zircon U-Pb age in overlying basalt	49° (Strik et al., 2003)	Basalt (Mt. Roe)	Macfarlane et al. (1994), XRF
Black Reef	2.71-2.59	2,714±8 zircon U-Pb age in underlying basalt (Venterstorp Fm.)	2,588±7 Ma zircon U-Pb age in overlying tuff (Oak Tree Fm.)	NA (age uncertain)	Hydrothermally altered granite	Maynard et al. (1995), XRF
Saganaga	2.685	2,6903±0.26 Ma zircon U-Pb age in parent	~2680 Ma inferred deformation age of overlying Ogishkemuncie Conglomerate	NA (rapid apparent polar wander)	Tonalite (Saganaga)	Driese et al. (2011), XRF
Lauzon Bay	2.45	~2.7-2.4 Ga K-Ar age in parent	~2,457 Ma youngest detrital zircon U-Pb age in overlying Matinenda Fm.	14° (Evans and Halls, 2010, from Matachewan dikes)	Granite (Algoman)	Sutton and Maynard (1992), XRF; New, ICP-MS
Pronto	2.45	~2.7-2.4 Ga K-Ar age in parent	~2,457 Ma youngest detrital zircon U-Pb age in overlying Matinenda Fm.	14° (ibid.)	Granite (Algoman)	Murakami et al. (2011), XRF
Denison	2.45	~2.7-2.4 Ga K-Ar age in	2,452.5±6.2 Ma zircon U-Pb	14° (ibid.)	Tonalite (Algoman)	Prasad and

		parent	age in overlying Copper Cliff rhyolite			Roscoe (1996), XRF
Quirke II	2.45	2,452.5±6.2 Ma zircon U-Pb age in Cooper Cliff rhyolite, correlative with parent	~2,457 Ma youngest detrital zircon U-Pb age in overlying Matinenda Fm.	14° (ibid.)	Diabase (Dollyberry)	Prasad and Roscoe (1991), XRF
Cooper Lake	2.45	2,452.5±6.2 Ma zircon U-Pb age in Cooper Cliff rhyolite, correlative with parent	~2,457 Ma youngest detrital zircon U-Pb age in overlying Matinenda Fm.	14° (ibid.)	Diabase (Dollyberry)	Babechuk et al. (2019), XRF
Ville Marie	2.25	2,290±90 Ma Rb-Sr age of underlying Gowganda Fm.	2,219±4 Ma ziron U-Pb age in overlying Nipissing Diabase	1° (Schmidt and Williams, 1999)	Granite (Ville Marie)	Rainbird et al. (1990), XRF
Hekpoort	2.1	2,193±71 Ma Rb-Sr age of parent	2,061±2 Ma zircon U-Pb age in overlying Rooiberg Group volcanics	NA (rapid APW)	Basalt (Hekpoort)	Beukes et al. (2002), XRF
Beaverlodge Lake	1.9	1,931±1 zircon U-Pb age of parent	1,906±1 zircon U-Pb age in overlying Zebulon Fm. volcanics	2-12° (Toma et al., 2019)	Feldspar ±quartz porphyry (Hottah)	Toma et al. (2019), ICP-AES
Flin Flon	1.85	1,900-1,880 Ma zircon U-Pb age range of parent	1,847±2 Ma youngest detrital zircon U-Pb age in overlying Missi Group	NA (arc terrane)	Hydrothermally altered basalt (Flin Flon Belt volcanics)	Babechuk and Kamber (2013), XRF
Baraboo	1.7	1,749±12 Ma zircon U-Pb age of parent	1,782-1,712 Ma detrital zircon U-Pb age range in overlying Baraboo Quartzite	60° (Kotzer et al., 1992, from correl. Manitou Falls Fm.)	Granite (Baxter Hollow)	Driese and Medaris (2008), XRF
Avontuur	1.25	2,426±3 Ma baddeleyite U-Pb age in underlying basalt (Ongeluk Fm.)	1,245±20 Ma zircon U-Pb age in overlying Mapedi Fm. tuff bed[2]	26° (Evans et al., 2002)	Diabase	Kock et al. (2020), XRF
Drakenstein	1.25	2,426±3 baddeleyite U-Pb age of parent[2]	1,245±20 Ma zircon U-Pb age in overlying Mapedi Fm. tuff bed[2]	26° (ibid.)	Basalt (Ongeluk Fm.)	Wiggering and Beukes (1990), XRF
Temperance River	1.097-1.094	1,097±2 Ma zircon U-Pb age in underlying Palisade Head Rhyolite	1,099-1,094 Ma zircon U-Pb age range of overlying Duluth complex	26° (Fairchild et al., 2017)	Basalt (North Shore Volcanic Group)	Sheldon (2013), XRF

Sigula	0.60-0.56	595-600 Ma zircon U-Pb age range of underlying basalt	558±1 Ma zircon U-Pb age in overlying Redkino volcanics	NA (rapid APW)	Metagabbro	Liivamägi et al. (2015), XRF
Roded	0.58-0.52	610-580 Ma zircon U-Pb age range of underlying dykes	Late early Cambrian biostratigraphic age of overlying Timna Fm.	NA (rapid APW)	Granite (Elat)	Sandler et al. (2012), ICP-OES
Timna	0.58-0.52	610-580 Ma zircon U-Pb age range of underlying dykes	Late early Cambrian biostratigraphic age of overlying Timna Fm.	NA (rapid APW)	Monzodiorite (Timna)	Sandler et al. (2012), ICP-OES
Verde River	>0.52	1,729±6 zircon U-Pb age in parent	Early Cambrian biostratigraphic age of overlying Tapeats Fm.	NA (possibly rapid APW)	Hydrothermally altered gabbro (Payson Ophiolite)	New, XRF
Elk Point	>0.503	1,733±2 Ma zircon U-Pb age in parent	503 Ma biostratigraphic age in overlying Bonneterre and Eau Clair Fms.	5° (Torsvik et al., 2012)	Metagabbro	Horodyskyj et al. (2012), ICP-AES
St. Francois Mtns.	>0.503	850-640 Ma zircon (U-Th)-He thermochronologic age for parent exhumation[3]	503 Ma biostratigraphic age in overlying Bonneterre and Eau Clair Fms.	5° (Torsvik et al., 2012)	Granite (Granite-Rhyolite Province)	New data, ICP-MS
Dunn Point	0.485-0.460	Early Ordovician biostratigraphic age in underlying Ferrona Fm.	460±3 Ma zircon U-Pb age in overlying rhyolite	40-60° (Hamilton and Murphy, 2004)	Basalt (Dunn Point Fm.)	Jutras et al. (2009), XRF
Boulder Creek	0.323-0.299	Bashkirian biostratigraphic age in regionally underlying Glen Eyrie Mbr.[4]	Gzhelian biostratigraphic age in overlying Fountain Fm.[4]	3-13° (Torsvik et al., 2012)	Granodiorite (Boulder Creek)	Condie et al. (1995), XRF
Ischigualasto	0.228	229±5 Ma K-Ar age in underlying Los Rastros Fm.	227.8±0.3 Ma sanidine Ar-Ar age in overlying Ischigualasto Fm.	48° S (Torsvik et al., 2012)	Basalt (Ischigualasto Fm.)	Tabor et al. (2004), ICP-OES
Bidar	0.0659	65.9±0.05 Ma zircon U-Pb age in entrained ashfall[5]	65.9±0.05 Ma (ashfall contemporaneous with soil formation)	28° S (Radhakrishna and Joseph, 2012)	Basalt (Ambenali Fm.)	Babechuk et al. (2014), XRF
Picture Gorge	0.166-0.163	16.572±0.018 Ma zircon U-Pb age in underlying Imnaha Basalt[5]	16.288±0.039 Ma zircon U-Pb age in overlying Grande Ronde Basalt[5]	45° N (Mankinen et al., 1987)	Basalt (Picture Gorge)	Sheldon (2003), XRF
Lower Rice	0.166-	16.572±0.018 Ma zircon U-	16.288±0.039 Ma zircon U-	46° N (ibid.)	Basalt (Grande Ronde,	Hobbs and Parrish

Creek	0.163	Pb age in underlying Imnaha Basalt[5]	Pb age in overlying Grande Ronde Basalt[5]		R1 unit)	(2016), XRF
Lawyer Canyon	0.166-0.163	16.572±0.018 Ma zircon U-Pb age in underlying Imnaha Basalt[5]	16.288±0.039 Ma zircon U-Pb age in overlying Grande Ronde Basalt[5]	46° N (ibid.)	Basalt (Grande Ronde, N1 unit)	Thomson et al. (2014), ICP-OES
Upper Shumaker	0.161-0.159	16.066±0.040 Ma zircon U-Pb age in underlying Vantage interbed[5]	15.895±0.019 Ma zircon U-Pb age in overlying Wanapum Basalt[5]	46° N (ibid.)	Basalt (Wanapum, Eckler Mtn Mbr.)	Thomson et al. (2014), ICP-OES

[1]Age constraint from Gumsley et al. (2013)
[2]Age constraints from Rasmussen et al. (2020).
[3]Age constraint from DeLucia et al. (2018)
[4]Age constraints from Sweet et al. (2015).
[5]Age constraints from Kasbohm and Schoene (2018).

Note: New ICP-MS data used in this analysis is for Mg only. ICP-MS data for Al and Ti are reported in Colwyn et al. (2019).

Abiogenic baseline calculations

Our method for determining an abiogenic baseline for weathering relates Al, Ti, and Mg loss in paleosols to relative percent losses determined experimentally by Hausrath et al. (2009). For each sample within a profile, we divided Mg percent loss relative to the parent by Mg percent loss over the duration of the experiment ($\Delta\%Mg_{exp}$) to produce a paleosol-specific amplification factor, A_{Mg}:

$$A_{Mg} = (Mg_{paleosol}/Mg_{parent} - 1) * 100 / \Delta\%Mg_{exp}$$

We then multiplied percent losses of Al and Ti in the experiment ($\Delta\%[Al,Ti]_{exp}$) by A_{Mg} to determine expected losses for these elements ($\Delta\%[Al,Ti]_{abio}$) if the parent material weathered under the same conditions as the experiment over the course of its formation:

$$\Delta\%[Al,Ti]_{abio} = A_{Mg} * \Delta\%[Al,Ti]_{exp}$$

Finally, we used these expected losses to calculate an expected $\tau_{Ti,Al}$ for each sample under abiogenic weathering:

$$\Delta Al/Ti_{abio} = (Al_{parent} * (100 - \Delta\%Al_{abio}) / Ti_{parent} * (100 - \Delta\%Ti_{abio})) / (Al/Ti)_{parent} - 1$$

Estimated *p*CO2 requirements for abiotic Al mobilization

Treating rainwater as a solution with zero total alkalinity gives the following relationship between pH and dissolved CO_2:

$$[CO_2]_{aq} = [H^+]^2 / k_1k_2, \text{ where } k_1k_2 = 4.25e^{-7} \text{ at } 25°C$$

Assuming rainwater is equilibrated with the atmosphere, the partial pressure of CO_2 in the atmosphere (pCO_2) can be determined with Henry's law:

$$pCO_2 = ([CO_2]_{aq} / k_H), \text{ where } k_H = 0.034 \text{ M/atm for } CO_2 \text{ at } 25°C$$

Assuming that aluminosilicate dissolution rates increase significantly below pH 4-5, the following are possible lower bounds for pCO_2 relative to the pre-industrial atmospheric level (PIAL, 280 ppm) necessary to mobilize Al in the absence of organic acids:

pCO_2 = 24.7x PIAL for pH 5

247x PIAL for pH 4.5

2470x PIAL for pH 4

Paleolatitude correlations

Estimated paleolatitudes in Supplementary Table 1 come from paleomagnetic pole measurements taken either directly from paleosols (e.g. the Drakenstein paleosol; Evans et al., 2002), from the parent (e.g. the Mt. Roe #2 paleosol; Strik et al., 2003), from overlying sediments (e.g. the Ville Marie paleosol; Schmidt and Williams, 1999), or from correlative rocks within the terrane that hosts the paleosol (e.g. the basal Huronian paleosols of the Superior Craton, including Lauzon Bay, Pronto, Denison, Quirke II, and Cooper Lake; Evans and Halls, 2010). In some cases, highly uncertain paleomagnetic poles from host terranes were replaced with poles from tectonically adjacent terranes. For example, the Hottah arc terrane, which hosts the 1.9 Ga Beaverlodge Lake paleosol, was likely close to accretion with the Slave Craton at the

time of paleosol formation. Likewise we do not report estimates for the 1.85 Ga Flin Flon paleosol, as tectonic relationships between the Flin Flon arc and its current nearest terranes, the Hearne and Superior cratons, are uncertain at 1.85 Ga (David Evans, personal communication). Lastly, we do not report latitudes for paleosols that formed during times of rapid apparent polar wander, as even moderate uncertainties in the age of paleosol formation will lead to significant uncertainties in pole positions.

Correlations between $\tau_{Ti,Al}$ values (means, minima, and maxima) and estimated paleolatitudes for paleosols are shown in Supplementary Figure 1. Paleolatitude estimates reported as ranges in Table 1 were converted to averages. Data were separated into positive and negative subsets to independently assess gain and loss, respectively.

Provenance tracers

An important criterion for effective provenance tracers in soils and paleosols is that they are relatively immobile, meaning that their relative abundance does not change with weathering. Another important criterion when using elements as tracers is that their abundance should vary considerably between rock types. Th and Zr satisfy both of these criteria and work well for distinguishing mafic from felsic sediment sources (Hallberg, 1984; McLennan et al., 1993). This means that Th/Zr ratios in soils and paleosols should match that of their parent if underlying rock is the single source of weatherable material.

One of the most common sources of added material in soils is wind-blown dust or ash, which may significantly offset mass loss during weathering (Porder et al., 2007). Within paleosols, up-profile enrichments in K and Rb have been cited as evidence for aeolian deposition given that dust and ash are often enriched in these elements relative to average continental crust (Sheldon, 2003). However, K enrichments in paleosols are more often linked to metasomatism, which is a post-depositional process (Fedo et al., 1995).

We produced cross plots of Rb vs. K in addition to Th vs. Zr to assess the possibility of allochthonous input to paleosols. Strong correlation between Rb and K suggests a single source of weatherable material, meaning that up-profile K enrichments are likely products of metasomatism rather than dust input. Interestingly some paleosols exhibit strong Rb-K but poor Th-Zr correlation. If scatter in Th-Zr space indicates mixture of multiple source materials, then corresponding scatter in Rb-K space would also be expected. Strong correlation instead suggests that K and Rb enrichments postdated soil formation and were probably associated with metasomatism (Supplementary Figure 2). Consequently, we do not consider K and Rb effective provenance tracers for paleosols.

Supplementary Figures

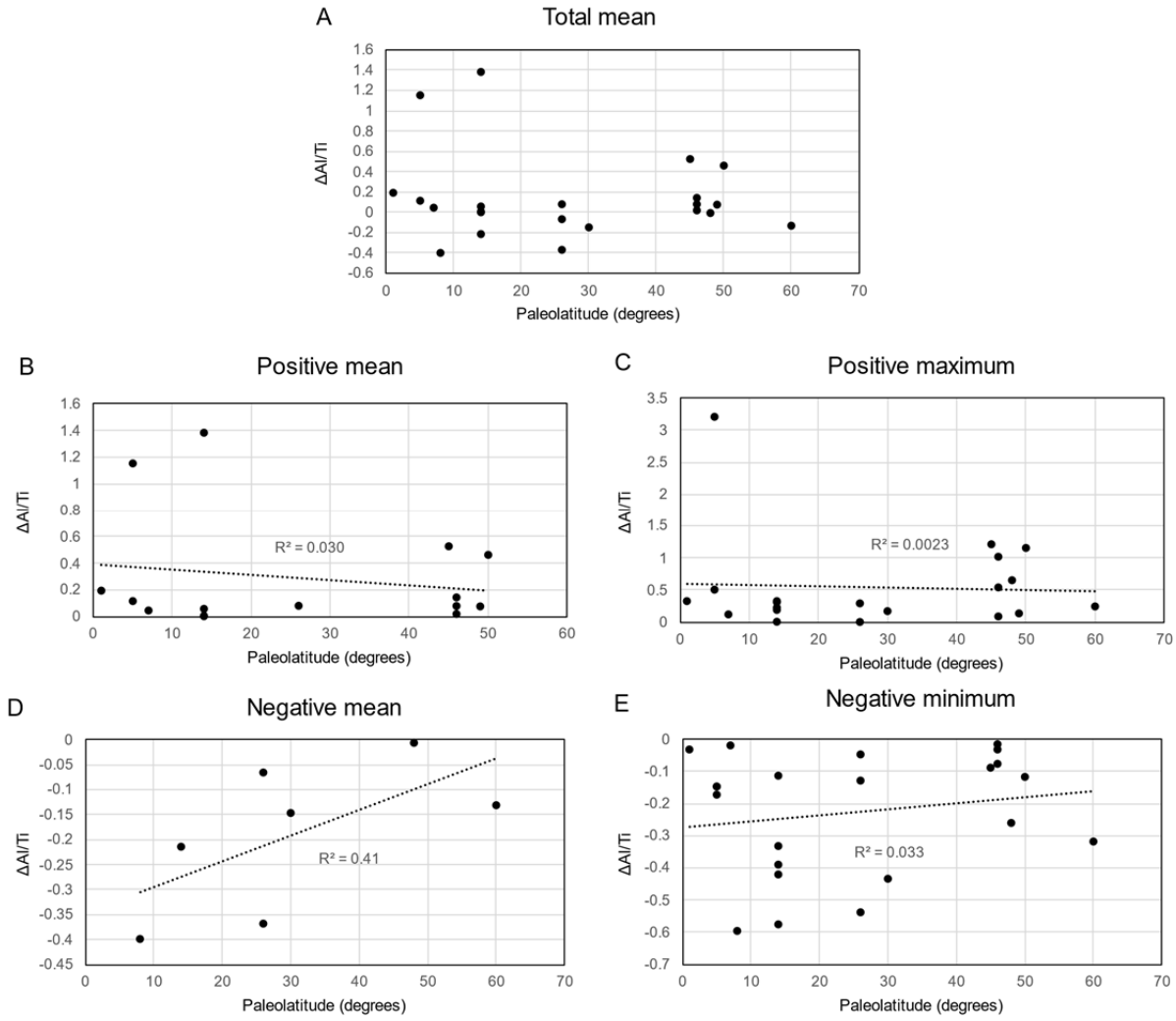

Supplementary Figure 1. Correlations between ΔAl/Ti and estimated paleolatitudes for paleosols. Positive minima and negative maxima are not shown due to a lack of data satisfying those conditions. All correlations demonstrate the expected inverse relationship between the magnitude of loss or gain and latitude, but this relationship is only weakly supported. Moreover, the most highly negative and positive ΔAl/Ti values are not confined to a discrete low-latitude belt, but vary continuously with latitude.

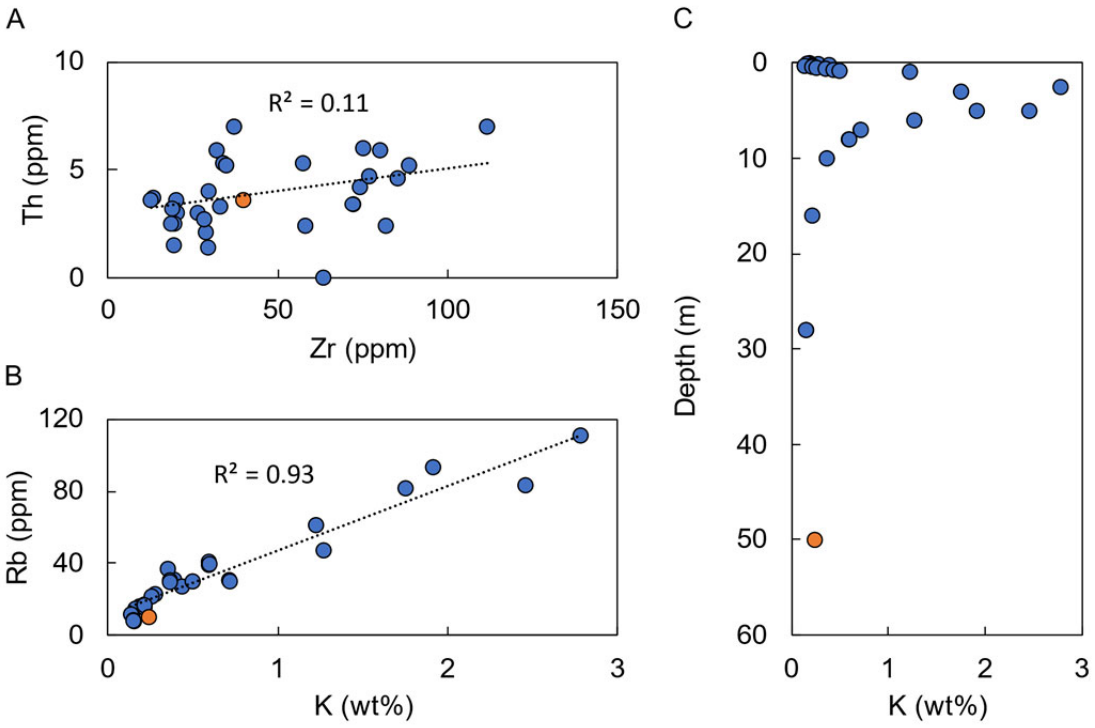

Supplementary Figure 2. Crossplots of Th-Zr (A) and Rb-K (B) in the Verde River paleosol. Poor correlation between Th and Zr indicate input and mixture of multiple sources of weatherable material despite strong correlation between Rb and K. This suggests Rb and K enrichments were likely post-depositional.

References

Alfimova, N.A., Felitsyn, S.B., and Matrenichev, V.A., 2011, Mobility of cerium in the 2.8-2.1 Ga exogenous environments of the Baltic Shield: Data on weathering profiles and sedimentary carbonates: Lithology and Mineral Resources, v. 46, p. 397, doi:10.1134/S0024490211050026.

Babechuk, M.G., and Kamber, B.S., 2013, The Flin Flon paleosol revisited: Canadian Journal of Earth Sciences, v. 50, p. 1223–1243, doi:10.1139/cjes-2013-0076.

Babechuk, M.G., Weimar, N.E., Kleinhanns, I.C., Eroglu, S., Swanner, E.D., Kenny, G.G., Kamber, B.S., and Schoenberg, R., 2019, Pervasively anoxic surface conditions at the onset of the Great Oxidation Event: New multi-proxy constraints from the Cooper Lake paleosol: Precambrian Research, v. 323, p. 126–163, doi:10.1016/j.precamres.2018.12.029.

Babechuk, M.G., Widdowson, M., and Kamber, B.S., 2014, Quantifying chemical weathering intensity and trace element release from two contrasting basalt profiles, Deccan Traps, India: Chemical Geology, v. 363, p. 56–75, doi:10.1016/j.chemgeo.2013.10.027.

Beukes, N.J., Dorland, H., Gutzmer, J., Nedachi, M., and Ohmoto, H., 2002, Tropical laterites, life on land, and the history of atmospheric oxygen in the Paleoproterozoic: Geology, v. 30, p. 491–494, doi:10.1130/0091-7613(2002)030<0491:TLLOLA>2.0.CO;2.

Colwyn, D.A., Sheldon, N.D., Maynard, J.B., Gaines, R., Hofmann, A., Wang, X., Gueguen, B., Asael, D., Reinhard, C.T., and Planavsky, N.J., 2019, A paleosol record of the evolution of Cr redox cycling and evidence for an increase in atmospheric oxygen during the Neoproterozoic: Geobiology, v. 17, p. 579–593, doi:10.1111/gbi.12360.

Condie, K.C., Dengate, J., and Cullers, R.L., 1995, Behavior of rare earth elements in a paleoweathering profile on granodiorite in the Front Range, Colorado, USA: Geochimica et Cosmochimica Acta, v. 59, p. 279–294, doi:10.1016/0016-7037(94)00280-Y.

DeLucia, M.S., Guenthner, W.R., Marshak, S., Thomson, S.N., and Ault, A.K., 2018, Thermochronology links denudation of the Great Unconformity surface to the supercontinent cycle and snowball Earth: Geology, v. 46, p. 167–170, doi:10.1130/G39525.1.

Driese, S.G., Jirsa, M.A., Ren, M., Brantley, S.L., Sheldon, N.D., Parker, D., and Schmitz, M., 2011, Neoarchean paleoweathering of tonalite and metabasalt: Implications for reconstructions of 2.69 Ga early terrestrial ecosystems and paleoatmospheric chemistry: Precambrian Research, v. 189, p. 1–17, doi:10.1016/j.precamres.2011.04.003.

Driese, S.G., and Medaris, L.G., 2008, Evidence for biological and hydrological controls on the development of a Paleoproterozoic paleoweathering profile in the Baraboo Range, Wisconsin, U.S.A.: Journal of Sedimentary Research, v. 78, p. 443–457, doi:10.2110/jsr.2008.051.

Evans, D.A.D., Beukes, N.J., and Kirschvink, J.L., 2002, Paleomagnetism of a lateritic paleoweathering horizon and overlying Paleoproterozoic red beds from South Africa: Implications for the Kaapvaal apparent polar wander path and a confirmation of atmospheric oxygen enrichment: Journal of Geophysical Research: Solid Earth, v. 107, p. EPM 2-1-EPM 2-22, doi:10.1029/2001JB000432.

Evans, D.A.D., and Halls, H.C., 2010, Restoring Proterozoic deformation within the Superior craton: Precambrian Research, v. 183, p. 474–489, doi:10.1016/j.precamres.2010.02.007.

Fairchild, L.M., Swanson-Hysell, N.L., Ramezani, J., Sprain, C.J., and Bowring, S.A., 2017, The end of Midcontinent Rift magmatism and the paleogeography of Laurentia: Lithosphere, v. 9, p. 117–133, doi:10.1130/L580.1.

Fedo, C.M., Nesbitt, H.W., and Young, G.M., 1995, Unraveling the effects of potassium metasomatism in sedimentary rocks and paleosols, with implications for paleoweathering conditions and provenance: Geology, v. 23, p. 921–924, doi:10.1130/0091-7613(1995)023<0921:UTEOPM>2.3.CO;2.

Gumsley, A.P., de Kock, M.O., Rajesh, H.M., Knoper, M.W., Söderlund, U., and Ernst, R.E., 2013, The Hlagothi Complex: The identification of fragments from a Mesoarchaean large igneous province on the Kaapvaal Craton: Lithos, v. 174, p. 333–348, doi:10.1016/j.lithos.2012.06.007.

Hallberg, J.A., 1984, A geochemical aid to igneous rock type identification in deeply weathered terrain: Journal of Geochemical Exploration, v. 20, p. 1–8, doi:10.1016/0375-6742(84)90085-2.

Hamilton, M.A., and Murphy, J.B., 2004, Tectonic significance of a Llanvirn age for the Dunn Point volcanic rocks, Avalon terrane, Nova Scotia, Canada: implications for the evolution of the Iapetus and Rheic Oceans: Tectonophysics, v. 379, p. 199–209, doi:10.1016/j.tecto.2003.11.006.

Hausrath, E.M., Neaman, A., and Brantley, S.L., 2009, Elemental release rates from dissolving basalt and granite with and without organic ligands: American Journal of Science, v. 309, p. 633–660, doi:10.2475/08.2009.01.

Hobbs, K.M., and Parrish, J.T., 2016, Miocene global change recorded in Columbia River basalt–hosted paleosols: GSA Bulletin, v. 128, p. 1543–1554, doi:10.1130/B31437.1.

Horodyskyj, L.B., White, T.S., and Kump, L.R., 2012, Substantial biologically mediated phosphorus depletion from the surface of a Middle Cambrian paleosol: Geology, v. 40, p. 503–506, doi:10.1130/G32761.1.

Jutras, P., Quillan, R.S., and LeForte, M.J., 2009, Evidence from Middle Ordovician paleosols for the predominance of alkaline groundwater at the dawn of land plant radiation: Geology, v. 37, p. 91–94, doi:10.1130/G25447A.1.

Kasbohm, J., and Schoene, B., 2018, Rapid eruption of the Columbia River flood basalt and correlation with the mid-Miocene climate optimum: Science Advances, v. 4, p. eaat8223, doi:10.1126/sciadv.aat8223.

Kock, M.O.D., Monareng, B.F., Blignaut, L., Smith, A.J.B., and Beukes, N.J., 2020, Geochemistry of Paleoproterozoic saprolite developed in diabase intruding the Hotazel Formation in the Avontuur deposit of the Kalahari Manganese Field, South Africa: South African Journal of Geology, doi:10.25131/sajg.123.0001.

Kotzer, T.G., Kyser, T.K., and Irving, E., 1992, Paleomagnetism and the evolution of fluids in the Proterozoic Athabasca Basin, northern Saskatchewan, Canada: Canadian Journal of Earth Sciences, v. 29, p. 1474–1491, doi:10.1139/e92-118.

Liivamägi, S., Somelar, P., Vircava, I., Mahaney, W.C., Kirs, J., and Kirsimäe, K., 2015, Petrology, mineralogy and geochemical climofunctions of the Neoproterozoic Baltic paleosol: Precambrian Research, v. 256, p. 170–188, doi:10.1016/j.precamres.2014.11.008.

Luskin, C., Wilson, A., Gold, D., and Hofmann, A., 2019, The Pongola Supergroup: Mesoarchaean Deposition Following Kaapvaal Craton Stabilization, *in* Kröner, A. and Hofmann, A. eds., The Archaean Geology of the Kaapvaal Craton, Southern Africa, Cham, Springer International Publishing, Regional Geology Reviews, p. 225–254, doi:10.1007/978-3-319-78652-0_9.

Macfarlane, A.W., Danielson, A., and Holland, H.D., 1994, Geology and major and trace element chemistry of late Archean weathering profiles in the Fortescue Group, Western Australia: implications for atmospheric PO2: Precambrian Research, v. 65, p. 297–317, doi:10.1016/0301-9268(94)90110-4.

Mankinen, E.A., Larson, E.E., Gromme, C.S., Prevot, M., and Coe, R.S., 1987, The Steens Mountain (Oregon) Geomagnetic Polarity Transition: 3. Its regional significance: Journal of Geophysical Research: Solid Earth, v. 92, p. 8057–8076, doi:10.1029/JB092iB08p08057.

Maynard, J.B., Sutton, S.J., Robb, L.J., Ferraz, M.F., and Meyer, F.M., 1995, A paleosol developed on hydrothermally altered granite from the hinterland of the Witwatersrand Basin: Characteristics of a source of basin fill: The Journal of Geology, v. 103, p. 357–377.

McLennan, S.M., Hemming, S., McDaniel, D.K., and Hanson, G.N., 1993, Geochemical approaches to sedimentation, provenance, and tectonics, *in* Geological Society of America Special Papers, Geological Society of America, v. 284, p. 21–40, doi:10.1130/SPE284-p21.

Murakami, T., Kasama, T., and Utsunomiya, S., 2011, Early Proterozoic weathering processes under low O_2 conditions reconstructed from a 2.45 Ga paleosol in Pronto, Canada: American Mineralogist, v. 96, p. 1613–1623, doi:10.2138/am.2011.3821.

Porder, S., Hilley, G.E., and Chadwick, O.A., 2007, Chemical weathering, mass loss, and dust inputs across a climate by time matrix in the Hawaiian Islands: Earth and Planetary Science Letters, v. 258, p. 414–427, doi:10.1016/j.epsl.2007.03.047.

Prasad, N., and Roscoe, S.M., 1996, Evidence of anoxic to oxic atmospheric change during 2.45-2.22 Ga from lower and upper sub-Huronian paleosols, Canada: Catena, v. 27, p. 105–121, doi:10.1016/0341-8162(96)00003-3.

Prasad, N., and Roscoe, S.M., 1991, Profiles of altered zones at ca. 2.45 Ga unconformities beneath Huronian strata, Elliot Lake, Ontario: Geological Survey of Canada Current Research Part C: Canadian Shield, p. 43–54.

Radhakrishna, T., and Joseph, M., 2012, Geochemistry and paleomagnetism of Late Cretaceous mafic dikes in Kerala, southwest coast of India in relation to large igneous provinces and mantle plumes in the Indian Ocean region: Geological Society of America Bulletin, v. 124, p. 240–255, doi:10.1130/B30288.1.

Rainbird, R.H., Nesbitt, H.W., and Donaldson, J.A., 1990, Formation and diagenesis of a sub-Huronian saprolith: Comparison with a modern weathering profile: The Journal of Geology, v. 98, p. 801–822, doi:10.1086/629455.

Rasmussen, B., Muhling, J.R., Zi, J.-W., Tsikos, H., and Fischer, W.W., 2020, A 1.25 Ga depositional age for the “Paleoproterozoic” Mapedi red beds, Kalahari manganese field, South Africa: New constraints on the timing of oxidative weathering and hematite mineralization: Geology, v. 48, p. 44–48, doi:10.1130/G46707.1.

Sandler, A., Teutsch, N., and Avigad, D., 2012, Sub-Cambrian pedogenesis recorded in weathering profiles of the Arabian-Nubian Shield: Sedimentology, v. 59, p. 1305–1320, doi:10.1111/j.1365-3091.2011.01307.x.

Schmidt, P.W., and Williams, G.E., 1999, Paleomagnetism of the Paleoproterozoic hematitic breccia and paleosol at Ville-Marie, Québec: further evidence for the low paleolatitude of Huronian glaciation: Earth and Planetary Science Letters, v. 172, p. 273–285, doi:10.1016/S0012-821X(99)00201-0.

Sheldon, N.D., 2013, Causes and consequences of low atmospheric pCO2 in the Late Mesoproterozoic: Chemical Geology, v. 362, p. 224–231, doi:10.1016/j.chemgeo.2013.09.006.

Sheldon, N.D., 2003, Pedogenesis and geochemical alteration of the Picture Gorge subgroup, Columbia River basalt, Oregon: GSA Bulletin, v. 115, p. 1377–1387, doi:10.1130/B25223.1.

Strik, G., Blake, T.S., Zegers, T.E., White, S.H., and Langereis, C.G., 2003, Palaeomagnetism of flood basalts in the Pilbara Craton, Western Australia: Late Archaean continental drift and the oldest known reversal of the geomagnetic field: Journal of Geophysical Research: Solid Earth, v. 108, doi:10.1029/2003JB002475.

Sutton, S.J., and Maynard, J.B., 1992, Multiple alteration events in the history of a sub-Huronian regolith at Lauzon Bay, Ontario: Canadian Journal of Earth Sciences, v. 29, p. 432–445, doi:10.1139/e92-038.

Sweet, D.E., Carsrud, C.R., and Watters, A.J., 2015, Proposing an Entirely Pennsylvanian Age for the Fountain Formation through New Lithostratigraphic Correlation along the Front Range: v. 52, p. 43–70.

Tabor, N.J., Montañez, I.P., Zierenberg, R., and Currie, B.S., 2004, Mineralogical and geochemical evolution of a basalt-hosted fossil soil (Late Triassic, Ischigualasto Formation, northwest Argentina): Potential for paleoenvironmental reconstruction: Geological Society of America Bulletin, v. 116, p. 1280–1293, doi:10.1130/B25222.1.

Thomson, B.J., Hurowitz, J.A., Baker, L.L., Bridges, N.T., Lennon, A.M., Paulsen, G., and Zacny, K., 2014, The effects of weathering on the strength and chemistry of Columbia River Basalts and their implications for Mars Exploration Rover Rock Abrasion Tool (RAT) results: Earth and Planetary Science Letters, v. 400, p. 130–144, doi:10.1016/j.epsl.2014.05.012.

Toma, J., Holmden, C., Shakotko, P., Pan, Y., and Ootes, L., 2019, Cr isotopic insights into ca. 1.9 Ga oxidative weathering of the continents using the Beaverlodge Lake paleosol, Northwest Territories, Canada: Geobiology, v. 17, p. 467–489, doi:10.1111/gbi.12342.

Torsvik, T.H. et al., 2012, Phanerozoic polar wander, palaeogeography and dynamics: Earth-Science Reviews, v. 114, p. 325–368, doi:10.1016/j.earscirev.2012.06.007.

Wiggering, H., and Beukes, N.J., 1990, Petrography and geochemistry of a 2000–2200-Ma-old hematitic Paleo-alteration profile on Ongeluk basalt of the Transvaal supergroup, Griqualand West, South Africa: Precambrian Research, v. 46, p. 241–258, doi:10.1016/0301-9268(90)90004-A.